

The Relativistic Dirac-Brueckner Approach to Asymmetric Nuclear Matter

E. N. E. van Dalen, C. Fuchs, and Amand Faessler
*Institut für Theoretische Physik, Universität Tübingen,
Auf der Morgenstelle 14, D-72076 Tübingen, Germany*

Abstract

The properties of asymmetric nuclear matter have been investigated in a relativistic Dirac-Brueckner-Hartree-Fock framework using the Bonn A potential. The components of the self-energies are extracted by projecting on Lorentz invariant amplitudes. Furthermore, the optimal representation scheme for the T matrix, the subtracted T matrix representation, is applied and the results are compared to those of other representation schemes. Of course, in the limit of symmetric nuclear matter our results agree with those found in literature. The binding energy E_b fulfills the quadratic dependence on the asymmetry parameter and the symmetry energy is 34 MeV at saturation density. Furthermore, a neutron-proton effective mass splitting of $m_n^* < m_p^*$ is found. In addition, results are given for the mean-field effective coupling constants.

PACS numbers: 21.65.+f, 21.60.-n, 21.30.-x, 24.10.Cn

I. INTRODUCTION

Symmetric nuclear matter has been studied extensively. The conventional nonrelativistic approach to nuclear matter, the BHF (Brueckner-Hartree-Fock) theory, goes back to earlier works by Brueckner and others [1, 2, 3, 4, 5, 6]. A breakthrough was achieved when the first relativistic (Dirac-) Brueckner-Hartree-Fock (DBHF) calculations were performed in the eighties [7, 8, 9]. It could describe remarkably successfully the saturation properties of nuclear matter, saturation energy and density of the equation of state (EOS).

Investigations of asymmetric nuclear matter, however, are rather rare. The breaking of isospin-symmetry complicates the problem considerably compared to symmetric or pure neutron matter. Some older studies within the nonrelativistic Brueckner scheme can be found in Refs. [10, 11]. In Ref. [12] a calculation in the nonrelativistic Brueckner scheme is presented for the Paris potential. Furthermore, the properties of isospin-asymmetric nuclear matter have been investigated in the framework of an extended nonrelativistic Brueckner approach in Ref. [13]. In addition, relativistic Brueckner calculations are performed in Ref. [14, 15, 16, 17, 18, 19, 20, 21]. Finally, we mention two calculations within the $\sigma - \omega$ model [22, 23].

The investigation of asymmetric matter is of importance for astrophysical studies such as the physics of supernova explosions [24] and of neutron stars [25], neutron-rich nuclei [26, 27], and their collisions [28]. The interest for the structure of neutron-rich nuclei and the collisions between these nuclei is only of recent date, because data for asymmetric nuclei were scarce in the past. However, this situation changes with recent advances in the development of high-intensity radioactive beam facilities that will produce nuclei with large neutron excess. Hence, systematic theoretical studies of asymmetric nuclear matter are becoming more important.

An important issue is the determination of the precise form of the nucleon self-energy. To determine the Lorentz structure and momentum dependence of the self-energy, the positive-energy-projected in-medium on-shell T matrix has to be decomposed into Lorentz invariant amplitudes. Because of the restriction to positive energy states ambiguities [29] arise, because pseudoscalar (ps) and pseudovector (pv) components can not uniquely be disentangled for on-shell scattering. However, with a pseudoscalar vertex the pion couples maximally to negative energy states which are not included in the standard Brueckner approach. This

coupling to negative energy states is inconsistent with the potentials used and leads to large and spurious nuclear self-energy contributions from negative energy states [30]. Hence, it was further demonstrated [31] that the conventional pv representation used to cure this problem fails. The reason is that pseudoscalar admixtures are still present. Finally, new and reliable methods, the complete pv representation [31] and the subtracted T matrix representation [32], were proposed to remove those spurious contributions from the T matrix for symmetric nuclear matter. In contrast, only the conventional pv representation has been applied for asymmetric nuclear matter [18].

In this work we describe asymmetric nuclear matter at zero temperature in the relativistic DBHF approach using the Bonn potential and their bare NN matrix elements V [33]. Furthermore, the optimal representation scheme for the T matrix, the subtracted T matrix representation, is applied. A comparison with other representation schemes is made, such as the ps representation, the conventional pv representation, and the complete pv representation. In addition, the relativistic Pauli operator is used. Compared to symmetric nuclear matter the theoretical and numerical effects are larger because protons and neutrons are occupying different Fermi spheres.

The plan of this paper is as follows. The relativistic DBHF is discussed in Sec. II. Furthermore, Sec. III is devoted to the covariant representation of the in-medium T matrix in connection with nucleon self-energy components. The results are presented and discussed in Sec. IV. Finally, we end with a summary and a conclusion in Sec. V.

II. RELATIVISTIC BRUECKNER APPROACH

In this section the relativistic Brueckner approach is discussed. First a short description of the relativistic Brueckner approach is given for symmetric nuclear matter. Next the modifications for the asymmetric case will be treated.

A. Symmetric Nuclear Matter

In the relativistic Brueckner approach the nucleon inside nuclear matter may be viewed as a dressed particle as a consequence of its two-body interaction with the surrounding nucleons. The in-medium interaction of the nucleons is treated in the ladder approximation

of the relativistic Bethe-Salpeter (BS) equation

$$T = V + i \int V Q G G T, \quad (1)$$

where T denotes the T matrix and V is the bare nucleon-nucleon interaction. The intermediate off-shell nucleons are described by a two-body propagator iGG . The Pauli operator Q accounts for the influence of the medium by the Pauli principle and prevents scattering to occupied states. The Green's function G which describes the propagation of dressed nucleons in the medium fulfills the Dyson equation

$$G = G_0 + G_0 \Sigma G. \quad (2)$$

G_0 denotes the free nucleon propagator while the influence of the surrounding nucleons is expressed by the self-energy Σ . In Brueckner formalism this self-energy is determined by summing up the interactions with all the nucleons inside the Fermi sea F in Hartree-Fock approximation

$$\Sigma = -i \int_F (Tr[GT] - GT). \quad (3)$$

The coupled set of Eqs. (1)-(3) represents a self-consistency problem and has to be iterated until convergence is reached. Below the approximations which are made in the standard relativistic Brueckner approach to solve the coupled set of Eqs. (1)-(3) are discussed.

1. Self-consistent spinor basis

Because of the requirement of translational and rotational invariance, hermiticity, parity conservation, and time reversal invariance, the most general form of the Lorentz structure of the self-energy in the nuclear matter rest frame is

$$\Sigma(k, k_F) = \Sigma_s(k, k_F) - \gamma_0 \Sigma_o(k, k_F) + \boldsymbol{\gamma} \cdot \mathbf{k} \Sigma_v(k, k_F), \quad (4)$$

The Σ_s , Σ_o , and Σ_v components are Lorentz scalar functions which actually depend on the Lorentz invariants $k^2, k \cdot j$ and j^2 , where j_μ denotes the baryon current. Hence, the Lorentz invariants can be expressed in terms of k_0 , $|\mathbf{k}|$ and k_F , where k_F denotes the Fermi momentum. The components of the self-energy are easily determined by taking the respective traces [8, 30]

$$\Sigma_s = \frac{1}{4} tr [\Sigma], \quad \Sigma_o = \frac{-1}{4} tr [\gamma_0 \Sigma], \quad \Sigma_v = \frac{-1}{4|\mathbf{k}|^2} tr [\boldsymbol{\gamma} \cdot \mathbf{k} \Sigma]. \quad (5)$$

The presence of the medium leads to effective masses and effective momenta of the nucleons

$$m^*(k, k_F) = M + \Re e \Sigma_s(k, k_F), \quad k^{*\mu} = k^\mu + \Re e \Sigma^\mu(k, k_F). \quad (6)$$

The Dirac equation written in terms of these effective masses and momenta has the form

$$[\gamma_\mu k^{*\mu} - m^*(k, k_F)]u(k, k_F) = 0. \quad (7)$$

In the following we will work in the quasi-particle approximation, i.e. the imaginary part of the self-energy $\Im m \Sigma$ will be neglected, to simplify the self-consistency scheme. To determine the self-energy only positive-energy states are needed in the relativistic Brueckner approach. Therefore, the full nucleon propagator can be replaced in Eq. (3) by the Dirac propagator [8, 34]

$$G_D(k, k_F) = [\gamma_\mu k^{*\mu} + m^*(k, k_F)]2\pi i \delta(k^{*2} - m^{*2}(k, k_F))\Theta(k^{*0})\Theta(k_F - |\mathbf{k}|). \quad (8)$$

Here k denotes the momentum of a nucleon inside the Fermi sea in the nuclear matter rest frame. This momentum is on mass shell. Due to the Θ -functions in the propagator only positive energy nucleons are allowed in the intermediate scattering states which eliminates the divergent contributions from negative energy states. Thus we avoid the delicate problem of infinities in the theory which generally will occur if one includes contributions from negative energy nucleons in the Dirac sea [8, 18, 35].

By the introduction of the reduced effective mass and kinetic momentum

$$\tilde{k}_\mu^* = k_\mu^* / (1 + \Sigma_v(k, k_F)), \quad \tilde{m}^*(k, k_F) = m^*(k, k_F) / (1 + \Sigma_v(k, k_F)), \quad (9)$$

the Dirac equation in the nuclear matter rest frame can be rewritten as

$$[\gamma_\mu \tilde{k}^{*\mu} - \tilde{m}^*(k, k_F)]u(k, k_F) = 0. \quad (10)$$

In general the reduced effective mass is density and momentum dependent. To simplify the calculation, however, the ‘‘reference spectrum approximation’’ [36] is applied in the iteration procedure, i.e. the effective mass of the nucleon is assumed to be entirely density dependent ($|\mathbf{k}| = k_F$). The method implies that the self-energy itself is only weakly momentum dependent. Therefore, at the end of the calculation one has to verify the consistency of the

assumption $\Sigma(k) \approx \Sigma(|\mathbf{k}| = k_F)$ with the result of the iteration procedure.

The solution of the Dirac equation in Eq. (10) provides the in-medium nucleon spinor

$$u_\lambda(k, k_F) = \sqrt{\frac{\tilde{E}^*(\mathbf{k}) + \tilde{m}_F^*}{2\tilde{m}_F^*}} \begin{pmatrix} 1 \\ \frac{2\lambda|\mathbf{k}|}{\tilde{E}^*(\mathbf{k}) + \tilde{m}_F^*} \end{pmatrix} \chi_\lambda, \quad (11)$$

where $\tilde{E}^*(\mathbf{k}) = \sqrt{\mathbf{k}^2 + \tilde{m}_F^{*2}}$ [56]. χ_λ denotes a two-component Pauli spinor with $\lambda = \pm\frac{1}{2}$. The normalization of the Dirac spinor is thereby chosen as $\bar{u}_\lambda(k, k_F)u_\lambda(k, k_F) = 1$. Since the spinor contains the reduced effective mass the matrix elements of the bare nucleon-nucleon interaction become density dependent. This density dependence, which is absent in nonrelativistic Brueckner calculations, is actually considered as the main reason for the success of the relativistic DBHF approach concerning the description of the nuclear saturation mechanism [7].

2. Covariant T matrix

We apply the relativistic Thompson equation [37] to solve the scattering problem of two nucleons in the nuclear medium. Therefore the two-particle propagator iGG in the BS equation, Eq. (1), has to be replaced by the effective Thompson propagator [37]. The Thompson propagator implies that the time-like component of the momentum transfer in V and T is set equal to zero which is a natural constraint in the c.m. frame, but not a covariant one. The Thompson propagator projects the intermediate nucleons onto positive energy states and restricts the exchanged energy transfer by $\delta(k^0)$ to zero. Thus Eq. (1) is reduced to a three-dimensional integral equation. In the two-particle center of mass (c.m.) frame - the natural frame for studying two-particle scattering processes - the Thompson equation can be written as [30, 38]

$$T(\mathbf{p}, \mathbf{q}, x)|_{c.m.} = V(\mathbf{p}, \mathbf{q}) + \int \frac{d^3\mathbf{k}}{(2\pi)^3} V(\mathbf{p}, \mathbf{k}) \frac{m_F^{*2}}{E^{*2}(\mathbf{k})} \frac{Q(\mathbf{k}, x)}{2E^*(\mathbf{q}) - 2E^*(\mathbf{k}) + i\epsilon} T(\mathbf{k}, \mathbf{q}, x), \quad (12)$$

where $\mathbf{q} = (\mathbf{q}_1 - \mathbf{q}_2)/2$ is the relative three-momentum of the initial state and \mathbf{k} and \mathbf{p} are the relative three-momenta of the intermediate and the final states, respectively. The Pauli operator Q depends on the boost three velocity \mathbf{u} into the c.m. frame. Hence, the T matrix depends on the set of parameters $x = \{k_F, m_F^*, |\mathbf{u}|\}$.

The Thompson equation (12) for the on-shell T matrix ($|\mathbf{p}| = |\mathbf{q}|$) can be solved applying standard techniques described in detail by Erkelenz [39]. Doing so, the positive-energy helicity T matrix elements are determined explicitly via the $|JMLS\rangle$ -scheme. In the on-shell case only five, for asymmetric nuclear matter six, of the sixteen helicity matrix elements are independent which follows from general symmetries [39]. After a partial wave projection onto the $|JMLS\rangle$ -states the integral reduces to an one-dimensional integral over the relative momentum $|\mathbf{k}|$ and Eq. (12) decouples into three subsystems of integral equations: the uncoupled spin singlet, the uncoupled spin triplet, and the coupled triplet states. To achieve the reduction to the one-dimensional integral equations the Pauli operator Q has to be replaced by an angle-averaged Pauli operator \overline{Q} [8]. Since the Fermi sphere is deformed to a Fermi ellipsoid in the two-nucleon c.m. frame, \overline{Q} is evaluated for such a Fermi ellipsoid:

$$\overline{Q} = \begin{cases} 0 & |\mathbf{k}| < k_{min} \\ \frac{\gamma E^*(k) - E_F^*}{\gamma u |\mathbf{k}|} & \text{for } k_{min} < |\mathbf{k}| < k_{max} \\ 1 & k_{max} < |\mathbf{k}| \end{cases} \quad (13)$$

with $k_{min} = \sqrt{k_F^2 - u^2 E_F^2}$, $k_{max} = \gamma(u E_F + k_F)$, and $u = |\mathbf{u}|$. The integral equations are solved by the matrix inversions techniques of Haftel and Tabakin [5].

The two-nucleon states are two-fermion states. Due to the anti-symmetry of these states the total isospin of the two-nucleon system ($I = 0, 1$) can be restored by the standard selection rule

$$(-1)^{L+S+I} = -1. \quad (14)$$

With help of Eqs. (3.28) and (3.32) in [39] the five independent partial wave amplitudes in the helicity representation are obtained from the five independent on-shell amplitudes in the $|JMLS\rangle$ -representation. The summation over the total angular momentum yields the five on-shell plane-wave helicity matrix elements

$$\langle \mathbf{p} \lambda'_1 \lambda'_2 | T^I(x) | \mathbf{q} \lambda_1 \lambda_2 \rangle = \sum_J \left(\frac{2J+1}{4\pi} \right) d_{\lambda'_1 \lambda_1}^J(\theta) \langle \lambda'_1 \lambda'_2 | T^{J,I}(\mathbf{p}, \mathbf{q}, x) | \lambda_1 \lambda_2 \rangle. \quad (15)$$

Here θ is the scattering angle between \mathbf{q} and \mathbf{p} , with $|\mathbf{p}| = |\mathbf{q}|$, while $\lambda = \lambda_1 - \lambda_2$ and $\lambda' = \lambda'_1 - \lambda'_2$. The reduced rotation matrices $d_{\lambda'_1 \lambda_1}^J(\theta)$ are those defined by Rose [40].

B. Asymmetric Nuclear Matter

In symmetric nuclear matter the Fermi momenta of protons and neutrons are equal. However, in asymmetric nuclear matter the protons and neutrons are occupying different Fermi spheres, leading to different Pauli operators and corresponding neutron and proton effective masses and self-energies. This asymmetry is also reflected in the fact that one has three different in-medium interactions of the nucleons. They are treated in the ladder approximation of the relativistic Bethe-Salpeter equation

$$T_{nn} = V_{nn} + i \int V_{nn} Q_{nn} G_n G_n T_{nn}, \quad (16)$$

$$T_{pp} = V_{pp} + i \int V_{pp} Q_{pp} G_p G_p T_{pp}, \quad (17)$$

$$T_{np}^{dir} = V_{np}^{dir} + i \int V_{np}^{dir} Q_{np} G_n G_p T_{np}^{dir} + i \int V_{np}^{exc} Q_{pn} G_p G_n T_{np}^{exc}, \quad (18)$$

and

$$T_{np}^{exc} = V_{np}^{exc} + i \int V_{np}^{exc} Q_{pn} G_p G_n T_{np}^{dir} + i \int V_{np}^{dir} Q_{np} G_n G_p T_{np}^{exc}, \quad (19)$$

where T_{ij} denotes one of the three different T matrices. The three different bare nucleon-nucleon interactions are described by one-boson exchange potentials V_{ij} . In the case of neutrons and protons having different effective masses, the helicity matrix elements cease to be symmetric under the exchange of these particles leading to an additional sixth independent helicity matrix element for the np interaction. These six independent amplitudes can be reduced to five, if one assumes an average mass in the np channel for V_{np} . In that case, V_{np}^{dir} is related to V_{np}^{exc} by the Fierz transformation, which would not be the case otherwise due to the unequal effective masses of neutrons and protons. Therefore, Eqs. (18) and (19) can be reduced to one equation,

$$T_{np} = V_{np} + i \int V_{np} Q_{np} G_n G_p T_{np}. \quad (20)$$

Next, the two-particle propagator $iG_i G_j$ has to be replaced by the effective propagator. In this work it is the Thompson propagator [37]. The effective Thompson propagator is given by

$$g_{ij} = iG_i G_j = \frac{m_i^* m_j^*}{E_i^* E_j^*} \frac{1}{\sqrt{s^*} - E_i^* - E_j^* + i\epsilon}, \quad (21)$$

where $\sqrt{s^*}$ is the invariant mass.

Furthermore, the Pauli operator Q has to be replaced by an angle-averaged Pauli operator \overline{Q} . The angle-averaged relativistic Pauli operators for the nn and pp interactions are identical to the one in the symmetric case which is given in Eq. (13). In contrast to the symmetric case, the Pauli operator for the np interaction has to be evaluated for Fermi ellipsoids with different sizes. The result for the angle-averaged Pauli operator \overline{Q}_{np} for asymmetric matter with a neutron excess is

$$\overline{Q}_{np} = \begin{cases} \Theta(\gamma u E_{Fn} - \gamma p_{Fn}) & |\mathbf{k}| < k_{min} \\ 1/2[\cos(\theta_p) - \cos(\theta_n)]\Theta(\theta_n - \theta_p) & \text{for } k_{min} < |\mathbf{k}| < k_{max} \\ 1 & k_{max} < |\mathbf{k}| \end{cases} \quad (22)$$

with $k_{min} = \gamma|uE_{Fn} - p_{Fn}|$, $k_{max} = \gamma(uE_{Fn} + p_{Fn})$,

$$\theta_p = \begin{cases} \arccos\left(\frac{\gamma E_p^*(k) - E_{Fp}^*}{\gamma|\mathbf{k}||\mathbf{u}|}\right) & \text{for } \left|\frac{\gamma E_p^*(k) - E_{Fp}^*}{\gamma|\mathbf{k}||\mathbf{u}|}\right| \leq 1 \\ 0 & \text{otherwise} \end{cases}, \quad (23)$$

and

$$\theta_n = \begin{cases} \arccos\left(\frac{E_{Fn}^* - \gamma E_n^*(k)}{\gamma|\mathbf{k}||\mathbf{u}|}\right) & \text{for } \left|\frac{E_{Fn}^* - \gamma E_n^*(k)}{\gamma|\mathbf{k}||\mathbf{u}|}\right| \leq 1 \\ \pi & \text{otherwise} \end{cases}. \quad (24)$$

However, the central quantities in the model are the neutron self-energy

$$\Sigma_n = -i \int_{F_n} (Tr[G_n T_{nn}] - G_n T_{nn}) - i \int_{F_p} (Tr[G_p T_{np}] - G_p T_{np}), \quad (25)$$

and the proton self-energy

$$\Sigma_p = -i \int_{F_p} (Tr[G_p T_{pp}] - G_p T_{pp}) - i \int_{F_n} (Tr[G_n T_{np}] - G_n T_{np}). \quad (26)$$

In Brueckner theory the integrations extend over the Fermi sea of the neutron F_n and of the proton F_p . Below, the expressions in Eqs. (25)-(26) will be specified for the different covariant representations.

III. COVARIANT REPRESENTATION AND THE SELF-ENERGY COMPONENTS

In this section we will consider four different representations of the T matrix: pseudoscalar, conventional pseudovector, complete pseudovector, and subtracted T matrix representation.

A. Pseudoscalar (*ps*) Representation

The nucleon self-energy components are calculated in the nuclear matter rest frame using the trace formulas, Eqs. (5). Since we determine the T matrix elements in the two-particle c.m. frame, a representation with covariant operators and Lorentz invariant amplitudes in Dirac space is the most convenient way to Lorentz-transform the T matrix from the two-particle c.m. frame into the nuclear matter rest frame [8]. On-shell a set of five linearly independent covariants is sufficient for such a T matrix representation in symmetric nuclear matter. A linearly independent, however, not unique set of five covariants is given by the following Fermi covariants

$$S = 1 \otimes 1, V = \gamma^\mu \otimes \gamma_\mu, T = \sigma^{\mu\nu} \otimes \sigma_{\mu\nu}, A = \gamma_5 \gamma^\mu \otimes \gamma_5 \gamma_\mu, P = \gamma_5 \otimes \gamma_5. \quad (27)$$

To circumvent the problem of unphysical contributions in the nucleon self-energy one uses antisymmetrized amplitudes $F_i^I(|\mathbf{p}|, \theta, x)$ and $F_i^I(|\mathbf{p}|, \pi - \theta, x)$. Thus, the representation of the T matrix is given by [30]

$$T^I(|\mathbf{p}|, \theta, x) = T^{I,dir}(|\mathbf{p}|, \theta, x) - T^{I,exc}(|\mathbf{p}|, \theta, x), \quad (28)$$

where the “direct” and “exchange” parts of the T matrix are defined as

$$T^{I,dir}(|\mathbf{p}|, \theta, x) = \frac{1}{2} \left[F_S^I(|\mathbf{p}|, \theta, x)S + F_V^I(|\mathbf{p}|, \theta, x)V + F_T^I(|\mathbf{p}|, \theta, x)T \right. \\ \left. + F_A^I(|\mathbf{p}|, \theta, x)A + F_P^I(|\mathbf{p}|, \theta, x)P \right], \quad (29)$$

and

$$T^{I,exc}(|\mathbf{p}|, \theta, x) = (-1)^{I+1} \frac{1}{2} \left[F_S^I(|\mathbf{p}|, \pi - \theta, x)\tilde{S} + F_V^I(|\mathbf{p}|, \pi - \theta, x)\tilde{V} \right. \\ \left. + F_T^I(|\mathbf{p}|, \pi - \theta, x)\tilde{T} + F_A^I(|\mathbf{p}|, \pi - \theta, x)\tilde{A} + F_P^I(|\mathbf{p}|, \pi - \theta, x)\tilde{P} \right], \quad (30)$$

where the interchanged invariants are defined as [41] $\tilde{S} = \tilde{S}S$, $\tilde{V} = \tilde{S}V$, $\tilde{T} = \tilde{S}T$, $\tilde{A} = \tilde{S}A$, and $\tilde{P} = \tilde{S}P$ with operator \tilde{S} exchanging particles 1 and 2, i.e. $\tilde{S}u(1)_\sigma u(2)_\tau = u(1)_\tau u(2)_\sigma$. Here \mathbf{p} and θ denote the relative three-momentum and the scattering angle between the scattered nucleons in the c.m. frame, respectively. In addition, the five Lorentz invariant amplitudes $F_i^I(|\mathbf{p}|, \theta, x)$ with $i = \{S, V, T, A, P\}$ depend also on $x = \{k_F, m_F^*, |\mathbf{u}|\}$. Taking the single nucleon momentum $\mathbf{k} = (0, 0, k)$ along the z -axis, we have for the scalar and

vector components of the neutron self-energy

$$\begin{aligned}\Sigma_s(\mathbf{k}) &= \frac{1}{4} \int_0^{k_{F_n}} \frac{d^3\mathbf{q}}{(2\pi)^3} \frac{m_n^*}{E_{q,n}^*} [4F_{\tilde{S}}^{nn} - F_{\tilde{S}}^{nn} - 4F_{\tilde{V}}^{nn} - 12F_{\tilde{T}}^{nn} + 4F_{\tilde{A}}^{nn} - F_{\tilde{P}}^{nn}] \\ &\quad + \frac{1}{4} \int_0^{k_{F_p}} \frac{d^3\mathbf{q}}{(2\pi)^3} \frac{m_p^*}{E_{q,p}^*} [4F_{\tilde{S}}^{np} - F_{\tilde{S}}^{np} - 4F_{\tilde{V}}^{np} - 12F_{\tilde{T}}^{np} + 4F_{\tilde{A}}^{np} - F_{\tilde{P}}^{np}],\end{aligned}\quad (31)$$

$$\begin{aligned}\Sigma_o(\mathbf{k}) &= \frac{1}{4} \int_0^{k_{F_n}} \frac{d^3\mathbf{q}}{(2\pi)^3} [-4F_{\tilde{V}}^{nn} + F_{\tilde{S}}^{nn} - 2F_{\tilde{V}}^{nn} - 2F_{\tilde{A}}^{nn} - F_{\tilde{P}}^{nn}] \\ &\quad + \frac{1}{4} \int_0^{k_{F_p}} \frac{d^3\mathbf{q}}{(2\pi)^3} [-4F_{\tilde{V}}^{np} + F_{\tilde{S}}^{np} - 2F_{\tilde{V}}^{np} - 2F_{\tilde{A}}^{np} - F_{\tilde{P}}^{np}],\end{aligned}\quad (32)$$

and

$$\begin{aligned}\Sigma_v(\mathbf{k}) &= \frac{1}{4} \int_0^{k_{F_n}} \frac{d^3\mathbf{q}}{(2\pi)^3} \frac{\mathbf{q} \cdot \mathbf{k}}{|\mathbf{k}|^2 E_{q,p}^*} [-4F_{\tilde{V}}^{nn} + F_{\tilde{S}}^{nn} - 2F_{\tilde{V}}^{nn} - 2F_{\tilde{A}}^{nn} - F_{\tilde{P}}^{nn}] \\ &\quad + \frac{1}{4} \int_0^{k_{F_p}} \frac{d^3\mathbf{q}}{(2\pi)^3} \frac{\mathbf{q} \cdot \mathbf{k}}{|\mathbf{k}|^2 E_{q,p}^*} [-4F_{\tilde{V}}^{np} + F_{\tilde{S}}^{np} - 2F_{\tilde{V}}^{np} - 2F_{\tilde{A}}^{np} - F_{\tilde{P}}^{np}].\end{aligned}\quad (33)$$

Corresponding expressions as in Eqs. (31)-(33) can be obtained for the components of the proton self-energy.

This representation gives a strong momentum dependence in the self-energy in the symmetric case [32]. This strong momentum dependence questions, of course, the validity of the 'reference spectrum approximation' used in the present self-consistency scheme. Furthermore, such a strong momentum dependence leads to unphysical results deep inside the Fermi sea since the effective mass drops to values which are close to zero. The strong momentum dependence of the self-energy [31] was found to originate mainly from the one-pion exchange contribution to the self-energy. Therefore, some representations which have a better treatment of the one-pion exchange contribution are given below.

B. Conventional Pseudovector (pv) Representation

As discussed in Sec. III A, the set of five covariants used to represent the on-shell T matrix is not uniquely defined as long as one works exclusively in the subspace of positive energy states [35]. Obviously, various alternative sets of five linearly independent covariants exist such as conventional pv representation. In this representation the pseudoscalar covariant $P = \gamma_5 \otimes \gamma_5$ in the T matrix representation in Eq. (28) is replaced by the pseudovector

covariant

$$\text{PV} = \frac{\gamma_5 \gamma_\mu q^\mu}{m_i^* + m_j^*} \otimes \frac{\gamma_5 \gamma_\mu q^\mu}{m_i^* + m_j^*} \quad (34)$$

with $q = p_1 - p_3$ and $q_0 = E_1 - E_3$. It leads to identical on-shell helicity matrix elements as the pseudoscalar covariant.

Using the pv representation of the T matrix as discussed above the nucleon self-energy becomes [30, 38]

$$\begin{aligned} \Sigma_s(\mathbf{k}) = & \frac{1}{4} \int_0^{k_{F_n}} \frac{d^3 \mathbf{q}}{(2\pi)^3} \frac{m_n^*}{E_{q,n}^*} [4F_S^{nn} - F_{\tilde{S}}^{nn} - 4F_{\tilde{V}}^{nn} - 12F_{\tilde{T}}^{nn} + 4F_{\tilde{A}}^{nn} \\ & + \frac{m_n^{*2} - k^{*\mu} q_\mu^*}{2m_n^{*2}} F_{\tilde{\text{PV}}}^{nn}] + \frac{1}{4} \int_0^{k_{F_p}} \frac{d^3 \mathbf{q}}{(2\pi)^3} \frac{m_p^*}{E_{q,p}^*} [4F_S^{np} - F_{\tilde{S}}^{np} - 4F_{\tilde{V}}^{np} \\ & - 12F_{\tilde{T}}^{np} + 4F_{\tilde{A}}^{np} + \frac{m_p^{*2} + m_n^{*2} - 2k^{*\mu} q_\mu^*}{(m_n^* + m_p^*)^2} F_{\tilde{\text{PV}}}^{np}], \end{aligned} \quad (35)$$

$$\begin{aligned} \Sigma_o(\mathbf{k}) = & \frac{1}{4} \int_0^{k_{F_n}} \frac{d^3 \mathbf{q}}{(2\pi)^3} [-4F_{\tilde{V}}^{nn} + F_{\tilde{S}}^{nn} - 2F_{\tilde{V}}^{nn} - 2F_{\tilde{A}}^{nn} \\ & - \frac{E_{k,n}^*}{E_{q,n}^*} \frac{m_n^{*2} - k^{*\mu} q_\mu^*}{2m_n^{*2}} F_{\tilde{\text{PV}}}^{nn}] + \frac{1}{4} \int_0^{k_{F_p}} \frac{d^3 \mathbf{q}}{(2\pi)^3} [-4F_{\tilde{V}}^{np} + F_{\tilde{S}}^{np} - 2F_{\tilde{V}}^{np} \\ & - 2F_{\tilde{A}}^{np} - \frac{2E_{k,n}^* (m_p^{*2} - k^{*\mu} q_\mu^*) - E_{q,p}^* (m_p^{*2} - m_n^{*2})}{E_{q,p}^* (m_n^* + m_p^*)^2} F_{\tilde{\text{PV}}}^{np}], \end{aligned} \quad (36)$$

and

$$\begin{aligned} \Sigma_v(\mathbf{k}) = & \frac{1}{4} \int_0^{k_{F_n}} \frac{d^3 \mathbf{q}}{(2\pi)^3} \frac{\mathbf{q} \cdot \mathbf{k}}{|\mathbf{k}|^2 E_{q,p}^*} [-4F_{\tilde{V}}^{nn} + F_{\tilde{S}}^{nn} - 2F_{\tilde{V}}^{nn} - 2F_{\tilde{A}}^{nn} \\ & - \frac{k_z}{q_z} \frac{m_n^{*2} - k^{*\mu} q_\mu^*}{2m_n^{*2}} F_{\tilde{\text{PV}}}^{nn}] + \frac{1}{4} \int_0^{k_{F_p}} \frac{d^3 \mathbf{q}}{(2\pi)^3} \frac{\mathbf{q} \cdot \mathbf{k}}{|\mathbf{k}|^2 E_{q,p}^*} [-4F_{\tilde{V}}^{np} + F_{\tilde{S}}^{np} \\ & - 2F_{\tilde{V}}^{np} - 2F_{\tilde{A}}^{np} - \frac{2k_z^* (m_p^{*2} - k^{*\mu} q_\mu^*) - q_z (m_p^{*2} - m_n^{*2})}{q_z (m_n^* + m_p^*)^2} F_{\tilde{\text{PV}}}^{np}]. \end{aligned} \quad (37)$$

The momentum dependence is still pronounced, because the pion contribution is not yet treated correctly as pseudovector as discussed in Ref. [31].

C. Complete Pseudovector (pv) Representation

Since Fierz transformation mixes the covariants in the conventional pv representation the HF nucleon self-energy is not reproduced when the pseudovector pion exchange potential is

used for the bare nucleon-nucleon interaction. Hence, to suppress the undesired pseudoscalar contribution of the pion to the nucleon self-energy we have to determine a different pv representation of the T matrix. To obtain a 'complete' pv representation the identities

$$\frac{1}{2}(T + \tilde{T}) = S + \tilde{S} + P + \tilde{P}, \quad (38)$$

$$V + \tilde{V} = S + \tilde{S} - P - \tilde{P} \quad (39)$$

are needed. Applying the operator identities (38)-(39) the "symmetrized" ps representation (28) can be rewritten as

$$\begin{aligned} T^I(|\mathbf{p}|, \theta, x) &= g_S^I(|\mathbf{p}|, \theta, x)S - g_{\tilde{S}}^I(|\mathbf{p}|, \theta, x)\tilde{S} + g_A^I(|\mathbf{p}|, \theta, x)(A - \tilde{A}) \\ &+ g_P^I(|\mathbf{p}|, \theta, x)P - g_{\tilde{P}}^I(|\mathbf{p}|, \theta, x)\tilde{P}, \end{aligned} \quad (40)$$

where the new amplitudes g_i^I are defined as

$$\begin{pmatrix} g_S^I \\ g_{\tilde{S}}^I \\ g_A^I \\ g_P^I \\ g_{\tilde{P}}^I \end{pmatrix} = \frac{1}{4} \begin{pmatrix} 4 & -2 & -8 & 0 & -2 \\ 0 & -6 & -16 & 0 & 2 \\ 0 & -2 & 0 & 0 & -2 \\ 0 & 2 & -8 & 4 & 2 \\ 0 & 6 & -16 & 0 & -2 \end{pmatrix} \begin{pmatrix} F_S^I \\ F_V^I \\ F_T^I \\ F_P^I \\ F_A^I \end{pmatrix}. \quad (41)$$

Due to the linear relations between the amplitudes F_i^I and g_i^I , the two ps representations (28) and (40) of the T matrix lead to identical results for the nucleon self-energy. When we replace in (40) the covariants P, \tilde{P} by the pseudovector covariants $PV, \tilde{P}\tilde{V}$, respectively, we arrive at the complete pv representation [41]

$$\begin{aligned} T^I(|\mathbf{p}|, \theta, x) &= g_S^I(|\mathbf{p}|, \theta, x)S - g_{\tilde{S}}^I(|\mathbf{p}|, \theta, x)\tilde{S} + g_A^I(|\mathbf{p}|, \theta, x)(A - \tilde{A}) \\ &+ g_{PV}^I(|\mathbf{p}|, \theta, x)PV - g_{\tilde{P}\tilde{V}}^I(|\mathbf{p}|, \theta, x)\tilde{P}\tilde{V}, \end{aligned} \quad (42)$$

with $g_{PV}^I(\theta)$ and $g_{\tilde{P}\tilde{V}}^I(\theta)$ being identical to $g_P^I(\theta)$ and $g_{\tilde{P}}^I(\theta)$, respectively. As shown in Ref. [31], this representation will be able to reproduce the Hartree-Fock results for the nucleon self-energy if we use the pseudovector pion exchange potential as bare nucleon-nucleon interaction. The self-energy components in the complete pv representation of the T matrix are given by

$$\begin{aligned} \Sigma_s(\mathbf{k}) &= \frac{1}{4} \int_0^{k_{Fn}} \frac{d^3\mathbf{q}}{(2\pi)^3} \frac{m_n^*}{E_{q,n}^*} [4g_S^{nn} - g_{\tilde{S}}^{nn} + 4g_A^{nn} + \frac{m_n^{*2} - k^{*\mu}q_\mu^*}{2m_n^{*2}} g_{PV}^{nn}] \\ &+ \frac{1}{4} \int_0^{k_{Fp}} \frac{d^3\mathbf{q}}{(2\pi)^3} \frac{m_p^*}{E_{q,p}^*} [4g_S^{np} - g_{\tilde{S}}^{np} + 4g_A^{np} + \frac{m_p^{*2} + m_n^{*2} - 2k^{*\mu}q_\mu^*}{(m_n^* + m_p^*)^2} g_{\tilde{P}\tilde{V}}^{np}], \end{aligned} \quad (43)$$

$$\begin{aligned} \Sigma_o(\mathbf{k}) = & \frac{1}{4} \int_0^{k_{Fn}} \frac{d^3 \mathbf{q}}{(2\pi)^3} [g_{\tilde{S}}^{nn} - 2g_A^{nn} - \frac{E_{k,n}^* m_n^{*2} - k^{*\mu} q_\mu^*}{E_{q,n}^* 2m_n^{*2}} g_{\tilde{P}\tilde{V}}^{nn}] \\ & + \frac{1}{4} \int_0^{k_{Fp}} \frac{d^3 \mathbf{q}}{(2\pi)^3} [g_{\tilde{S}}^{np} - 2g_A^{np} - \frac{2E_{k,n}^* (m_p^{*2} - k^{*\mu} q_\mu^*) - E_{q,p}^* (m_p^{*2} - m_n^{*2})}{E_{q,p}^* (m_n^* + m_p^*)^2} g_{\tilde{P}\tilde{V}}^{np}], \end{aligned} \quad (44)$$

and

$$\begin{aligned} \Sigma_v(\mathbf{k}) = & \frac{1}{4} \int_0^{k_{Fn}} \frac{d^3 \mathbf{q}}{(2\pi)^3} \frac{\mathbf{q} \cdot \mathbf{k}}{|\mathbf{k}|^2 E_{q,p}^*} [g_{\tilde{S}}^{nn} - 2g_A^{nn} - \frac{k_z m_n^{*2} - k^{*\mu} q_\mu^*}{q_z 2m_n^{*2}} g_{\tilde{P}\tilde{V}}^{nn}] \\ & + \frac{1}{4} \int_0^{k_{Fp}} \frac{d^3 \mathbf{q}}{(2\pi)^3} \frac{\mathbf{q} \cdot \mathbf{k}}{|\mathbf{k}|^2 E_{q,p}^*} [g_{\tilde{S}}^{np} - 2g_A^{np} \\ & - \frac{2k_z^* (m_p^{*2} - k^{*\mu} q_\mu^*) - q_z (m_p^{*2} - m_n^{*2})}{q_z (m_n^* + m_p^*)^2} g_{\tilde{P}\tilde{V}}^{np}]. \end{aligned} \quad (45)$$

However, as already pointed out in [31], this representation will not reproduce HF nucleon self-energy if other meson exchange potentials than pion exchange potentials are used.

D. Subtracted T Matrix Representation

The complete pv representation treated in Sect. III C will fail to reproduce the HF nucleon self-energy if other meson exchange potentials are applied than π - and (η -) mesons as bare interaction. Since the influence of the pion is dominantly given by the single-pion exchange, it should be reasonable to treat the bare interaction of the η and especially of the pion separately to the rest. After subtraction of the bare interaction of the η - and π -meson $V_{\pi,\eta}$, the remainder is the subtracted T matrix,

$$T_{Sub} = T - V_{\pi,\eta}. \quad (46)$$

The ps representation should be more appropriate for the subtracted T matrix because then the higher order contributions of the other meson exchange potentials are not treated incorrectly as pseudovector. Thus one chooses the complete pv representation for $V_{\pi,\eta}$ and the ps representation for the T_{Sub} to get the most favorable representation.

IV. RESULTS AND DISCUSSION

In Fig. 1 we present the results for the equation of state for various values of the proton fraction $Y_p = n_p/n_B$ using the Bonn A potential. The applied representations are the complete pv and the subtracted T matrix representation. The two extreme cases are symmetric

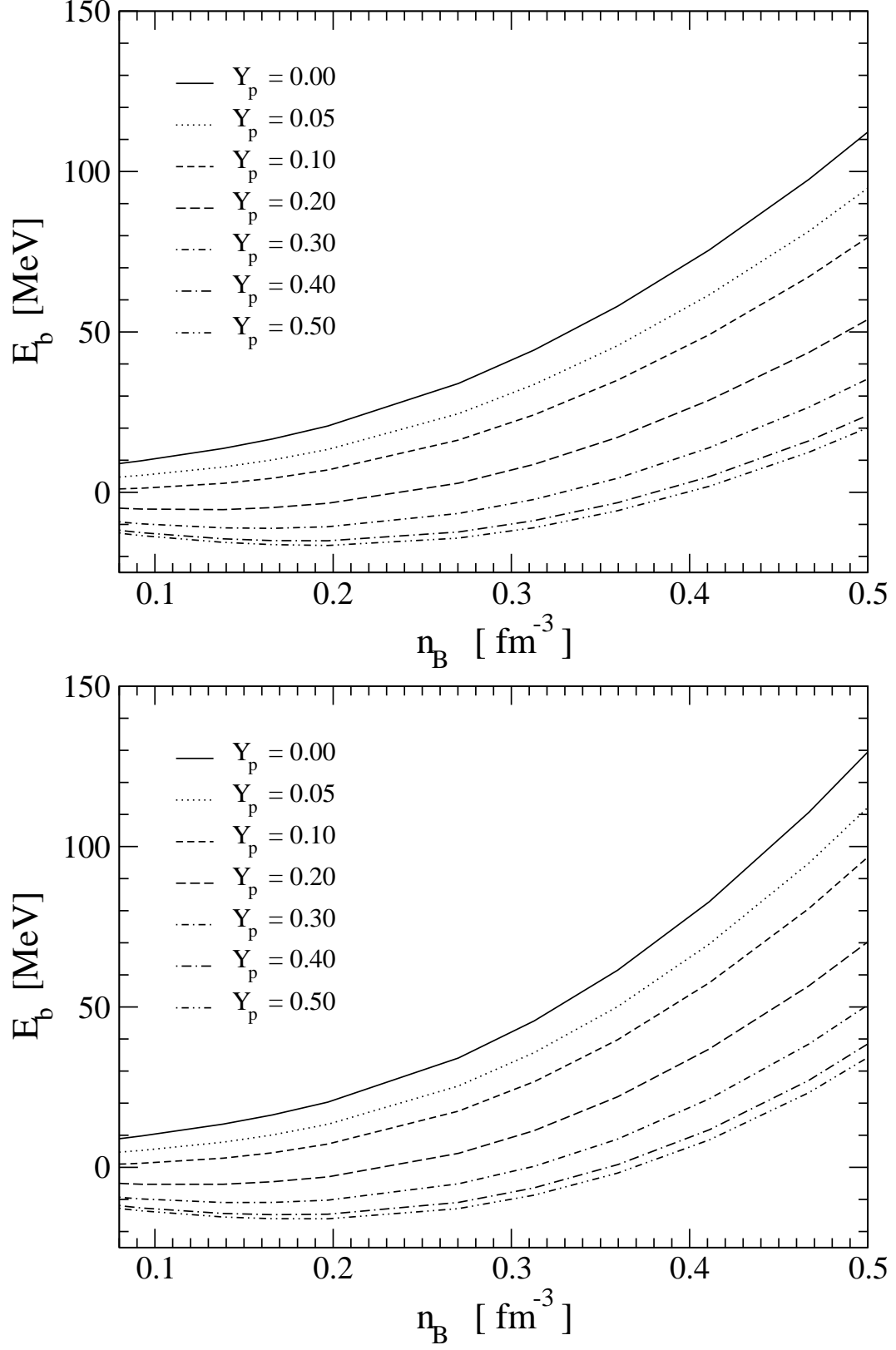


FIG. 1: Binding energy as a function of the baryon density for proton fractions Y_p ranging from 0 to 0.5. The complete pv (top) and subtracted T matrix representation (bottom) are used.

nuclear matter ($Y_p = 0.5$) and neutron matter ($Y_p = 0$). The symmetric nuclear matter results agree with those of Ref. [32]. The binding energy curves for intermediate values of Y_p lie between these two extreme curves. In addition to that, the binding energy E_b shows a nearly quadratic dependence on the asymmetry parameter $\beta = Y_n - Y_p$ in both representations. Furthermore, the symmetry energy is defined with help of the binding energy E_b as

$$E_{\text{sym}}(n_B) = \frac{1}{2} \left[\frac{\partial^2 E_b(n_B, \beta)}{\partial \beta^2} \right]_{\beta=0}. \quad (47)$$

Due to the nearly quadratic dependence of the binding energy on the asymmetry parameter, the symmetry energy can be equivalently calculated as

$$E_{\text{sym}}(n_B) = E_b(n_B, \beta = 1) - E_b(n_B, \beta = 0). \quad (48)$$

In Table I the calculated symmetry energy is given at saturation density for each repre-

representation	$k_F[\text{fm}^{-1}]$	$E_{\text{sym}} [\text{MeV}]$
conventional pv	1.41	30.80
complete pv	1.42	36.74
subtracted T matrix	1.39	34.36

TABLE I: The symmetry energy at saturation density for various representations. The Bonn A potential is used.

sentation. To compare the results in Table I, some values from literature are given below. The symmetry energy is found to be 25 MeV using the Groningen potential [18], whereas using the Bonn C potential [33] it is found to be 28 MeV. In this context it is worth to mention that in Ref. [18] the conventional pv representation was used for the decomposition of the T -matrix into Lorentz invariants. The result which the authors of [18] find for Bonn C is close to the present value obtained for Bonn A adopting the same projection scheme. However, the conventional pv representation suffers from on-shell ambiguities which lead to large and spurious contributions for the OPE. Thus we will omit this type of representation in the following. On the other hand, in Ref. [18] a sixth amplitude was introduced which appears only in the np channel for the case of different neutron and proton masses. For the two limiting cases, i.e. symmetric matter and pure neutron matter, this amplitude vanishes

identically. Hence the results for the symmetry energy are not affected by this additional amplitude. As discussed in [18], the definition of this amplitude is, however, not unique. Since we use an averaged neutron-proton mass for the evaluation of the V_{np} matrix elements as required by the Bonn code, we work, in contrast to Ref. [18], standardly with five amplitudes.

A recent liquid drop model calculation gives a result of 32.65 MeV [42]. A recent analysis of isovector giant dipole resonance (GDR) data within relativistic mean-field (RMF) theory set a range of $34 \leq E_{sym} \leq 36$ MeV [43]. Hence, in the complete pv representation the result for the symmetry energy in Table I is probably too high. The calculation, based on the subtracted T matrix projection scheme, yields a symmetry energy consistent with the empirical value. The value of 34 MeV is also in remarkable agreement with a recent approach to the nuclear many-body problem based on chiral dynamics in combination with QCD sum rules [44]. One has, however, to keep in mind that the saturation density obtained with Bonn A is slightly higher than the empirical value. Bonn A comes nevertheless closest towards the empirical values since Bonn B and C yield smaller densities but at the same time significantly too small binding energies [9, 32]. The comparison performed in [44] required therefore a rescaling of the DBHF results in order to adjust the densities. The symmetry energy does not change dramatically, i.e. at $n_B = 0.17 \text{ fm}^{-3}$ the values are 33 MeV (subtracted T matrix) and 34 MeV (complete pv).

The density dependence of the symmetry energy is shown in Fig. 2. It is similar as, e.g. found in the DBHF calculations of [21]. Although the EOS for symmetric matter is relatively soft ($K=230$ MeV, subtracted T matrix) the isospin dependence, respectively the symmetry energy, is stiff, in particular at high densities. As generally found in relativistic calculations it is significantly stiffer than in non-relativistic BHF approaches [12]. The dependence on the representation, i.e. complete pv or subtracted T matrix, is weak. For a quantitative comparison with mean-field phenomenology we compare E_{sym} in Fig. 2 also to a phenomenological results obtained recently within the framework of density dependent relativistic mean-field theory [43]. The asymmetry parameter a_4 is thereby varied from 30 to 38 MeV. At moderate densities the dependence of E_{sym} is qualitatively similar to the relativistic mean-field parameterizations using $a_4 = 32 - 34$ MeV. However, the density dependence of E_{sym} is generally more complex than in RMF theory. In particular at high densities E_{sym} shows a non-linear and more pronounced increase. For this comparison we

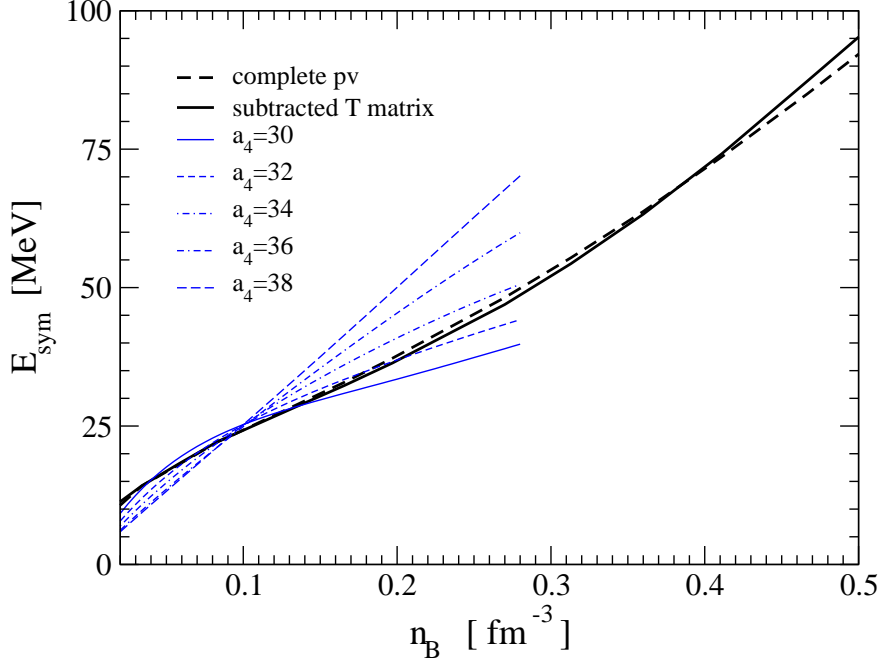


FIG. 2: Symmetry energy as a function of the baryon density. The complete pv and subtracted T matrix representation are used. In addition parameterizations from density dependent relativistic mean-field theory [45] are shown where the asymmetry parameter a_4 is varied from 30 to 38 MeV.

have chosen the parameter set from [45] which was obtained at equivalent compression moduli ($K=230$ MeV) although the authors of [45] favor a slightly higher incompressibility for the symmetric case.

In Fig. 3 the neutron effective mass is plotted as a function of the proton fraction Y_p for different representations at $n_B = 0.166 \text{ fm}^{-3}$. As already observed in the symmetric case [32], the magnitude of the self-energy, respectively of the effective mass, depends crucially on the projection scheme which is used for the T matrix. However, observables like the single-particle potential which are determined by the difference of scalar and vector self-energy components are much less affected by the different possible projection schemes since these effects cancel in leading order. Here we find that the neutron effective mass decreases for the ps representation with increasing proton fraction. This behavior is, however, an artefact of the ps representation which disappears when a proper decomposition of the T matrix is used. Mainly due to a relative large scalar amplitude in the direct part of the T matrix in the nn channel compared to that in the np channel, the neutron effective mass increases for the conventional pv , the complete pv , and the subtracted T matrix representation with

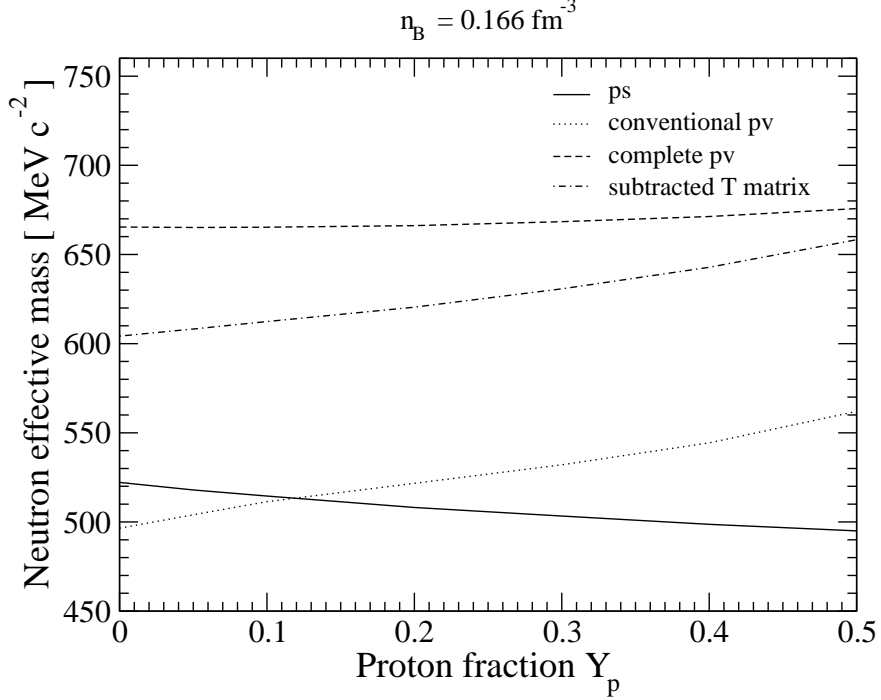


FIG. 3: Neutron effective mass as a function of the proton fraction at $n_B = 0.166 \text{ fm}^{-3}$ for different representations of the T matrix.

increasing proton fraction. In Fig. 4 the neutron effective mass is plotted as a function of the baryon density n_B for various values of the proton fraction using the subtracted T matrix representation. Of course, a strong density dependence can be observed. In addition, the proton fraction influences the neutron effective mass. The upmost curve is the symmetric nuclear matter curve, while the lowest curve is the neutron matter curve. The symmetric nuclear matter curve is in agreement with the results of Ref. [32]. For intermediate values of the proton fraction Y_p the curve lies between these two extreme curves.

A quantity which is sensitive on the momentum dependence of $\Sigma_{s,0,v}$ is the optical potential which a nucleon feels inside the nuclear medium. The optical potential is given by

$$U(|\mathbf{k}|, k^0) = \Sigma_s(|\mathbf{k}|) - \frac{1}{M} k^\mu \Sigma_\mu(|\mathbf{k}|) + \frac{\Sigma_s^2(|\mathbf{k}|) - \Sigma_\mu^2(|\mathbf{k}|)}{2M}. \quad (49)$$

The strength of the isovector nucleon optical potential, i.e., the Lane potential in [46], can be extracted from $(U_n - U_p)/(2\beta)$ at saturation density with $\beta = Y_n - Y_p$. From a large number of nucleon-nucleus scattering experiments at beam energies below about 100

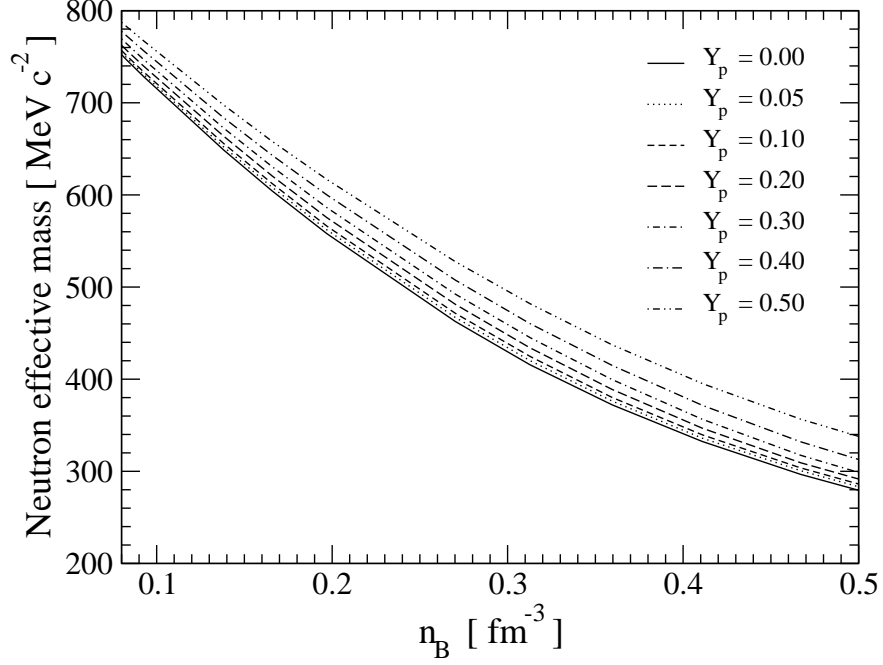


FIG. 4: Neutron effective mass as a function of the baryon density for proton fractions Y_p ranging from 0 to 0.5 using the subtracted T matrix representation.

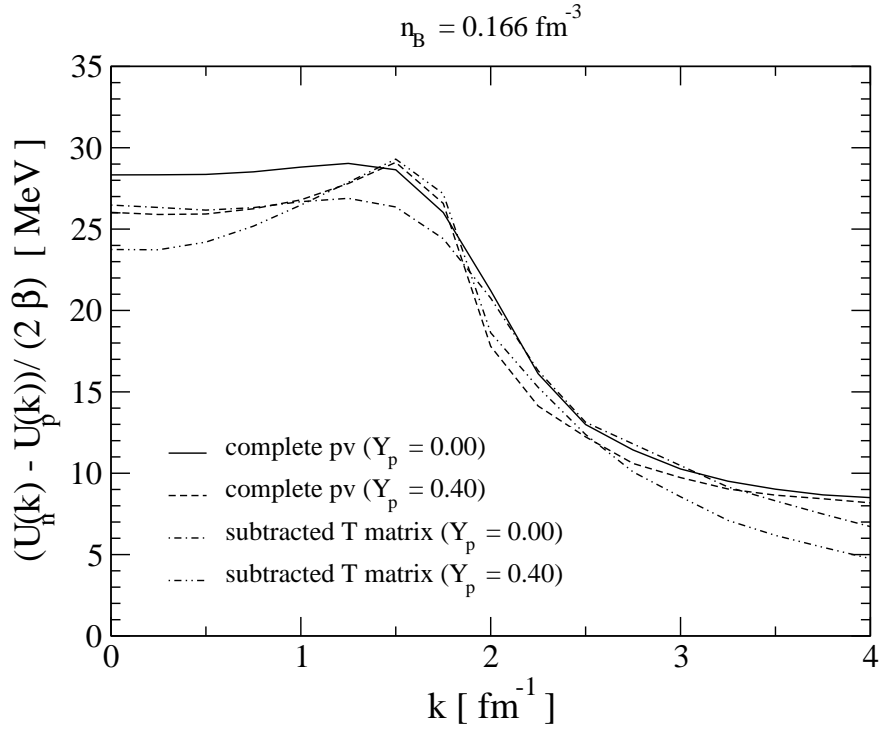


FIG. 5: Strength of the isovector potential at $n_B = 0.166 \text{ fm}^{-3}$ as a function of momentum \mathbf{k} .

MeV [47, 48, 49, 50] it can be concluded that this potential decreases with energy. The isovector nucleon optical potentials calculated for the complete pv and subtracted T matrix representation are shown in Fig. 5. In these cases the optical potential in neutron rich matter stays roughly constant up to a momentum of 1.5 fm^{-1} , corresponding to a kinetic energy of $E_{kin} \sim 45 \text{ MeV}$, and then decreases strongly with energy. In mean-field approximation, i.e. assuming momentum independent self-energy components, the behavior is different resulting in a continuously increasing optical isovector potential [57]. In the present case the decrease is caused by a pronounced explicit momentum dependence of the scalar and vector isovector self-energy components. The optical isovector potential $(U_n - U_p)/(2\beta)$ at zero momentum is in good agreement with the empirical value of 22 - 34 MeV [46]. Hence, the empirical isovector potential extracted from proton-nucleus scattering is well reproduced by the present calculation. The DBHF model predicts thereby neutron-proton effective mass splitting of $m_n^* < m_p^*$. The same behavior has been found in [18]. These facts stand in contradiction with the conclusion drawn in Ref. [46] which are based on nonrelativistic considerations. The same holds if one compares to nonrelativistic Brueckner calculations for asymmetric nuclear matter which predict an opposite behavior of the neutron-proton mass splitting than their relativistic counterparts. In this context one should, however, be aware that nonrelativistic approaches determine usually the effective Landau mass,

$$m_{NR}^* = \left[\frac{1}{M} + \frac{dU}{|\mathbf{k}| d|\mathbf{k}|} \right]_{|\mathbf{k}|=k_F}^{-1}, \quad (50)$$

which is in general not identical with the Dirac mass (6). Only in the limit of a constant, i.e. momentum independent self-energy including a vanishing spatial component Σ_v , both quantities coincide to leading order in the expansion of the relativistic single-particle energy if - in addition - the nonrelativistic single-particle potential shows a parabolic momentum dependence. However, the relativistic self-energy is in general momentum dependent and also the nonrelativistic potential is more complex [51].

The mean-field effective coupling constants can be obtained from the scalar and vector self-energies. Such coupling functions parameterize the correlations of the T-matrix in a handable way. They can be applied to finite nuclei within the framework of relativistic density dependent mean-field theory [52]. The four channels are: Dirac scalar isoscalar, Dirac vector isoscalar, Dirac scalar isovector, and Dirac vector isovector channel. The neutron and proton self-energies, respectively, are calculated at their Fermi momentum. Effective

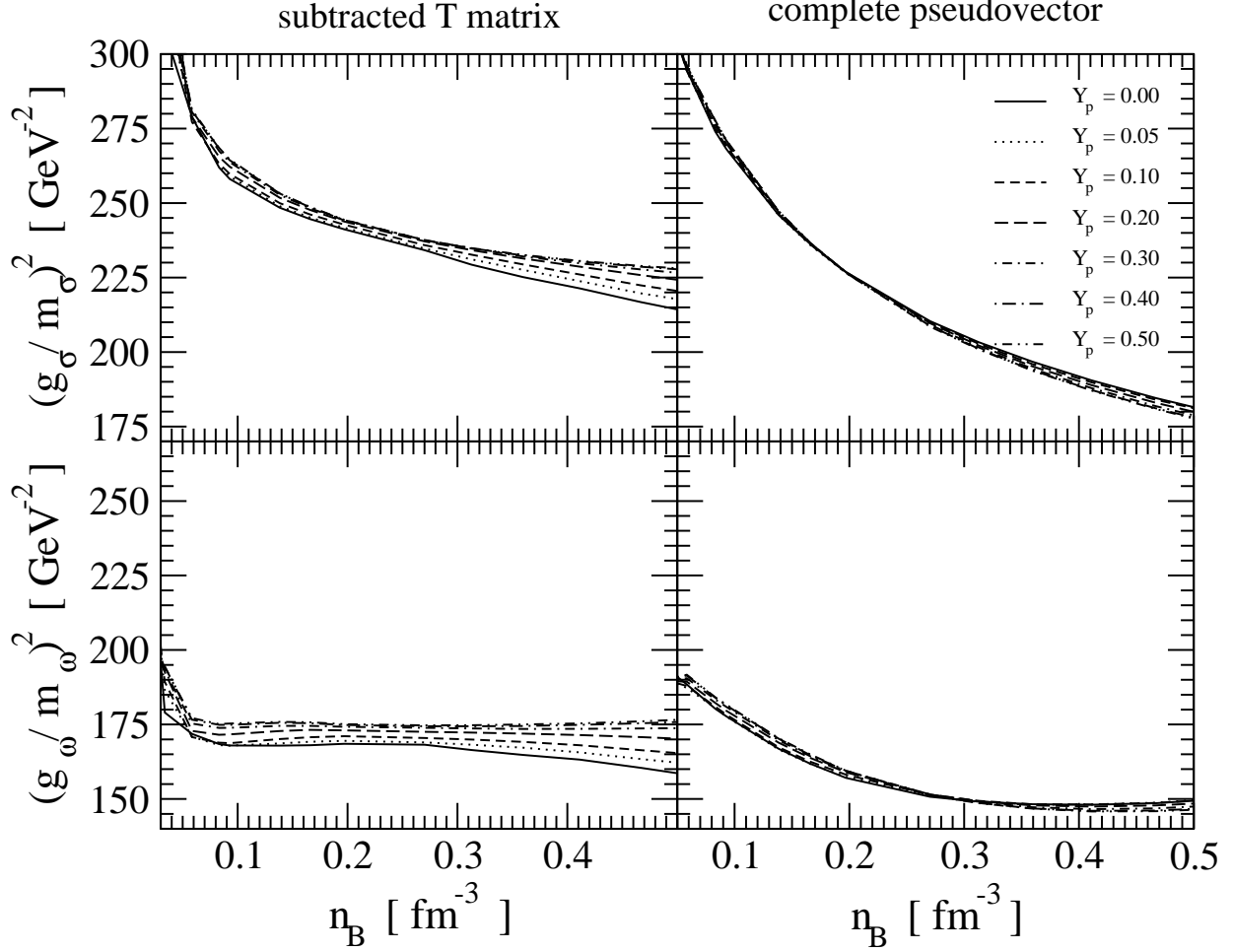


FIG. 6: The effective coupling constants in the isoscalar scalar g_σ and vector g_ω as a function of the baryon density for proton fractions Y_p ranging from 0 to 0.5 using the complete pv and subtracted T matrix representation.

coupling constants are then given by

$$\left(\frac{g_\sigma}{m_\sigma}\right)^2 = -\frac{1}{2} \frac{\Sigma_{s,n}(p_{Fn}) + \Sigma_{s,p}(p_{Fp})}{n_n^s + n_p^s}, \quad (51)$$

$$\left(\frac{g_\omega}{m_\omega}\right)^2 = -\frac{1}{2} \frac{\Sigma_{o,n}(p_{Fn}) + \Sigma_{o,p}(p_{Fp})}{n_n^v + n_p^v}, \quad (52)$$

$$\left(\frac{g_\delta}{m_\delta}\right)^2 = -\frac{1}{2} \frac{\Sigma_{s,n}(p_{Fn}) - \Sigma_{s,p}(p_{Fp})}{n_n^s - n_p^s}, \quad (53)$$

$$\left(\frac{g_\rho}{m_\rho}\right)^2 = -\frac{1}{2} \frac{\Sigma_{o,n}(p_{Fn}) - \Sigma_{o,p}(p_{Fp})}{n_n^v - n_p^v}, \quad (54)$$

where n_i^s and n_i^v are the scalar and vector densities [34]. The results for the isoscalar and isovector coupling constants are plotted in Figs. 6 and 7, respectively. The representa-

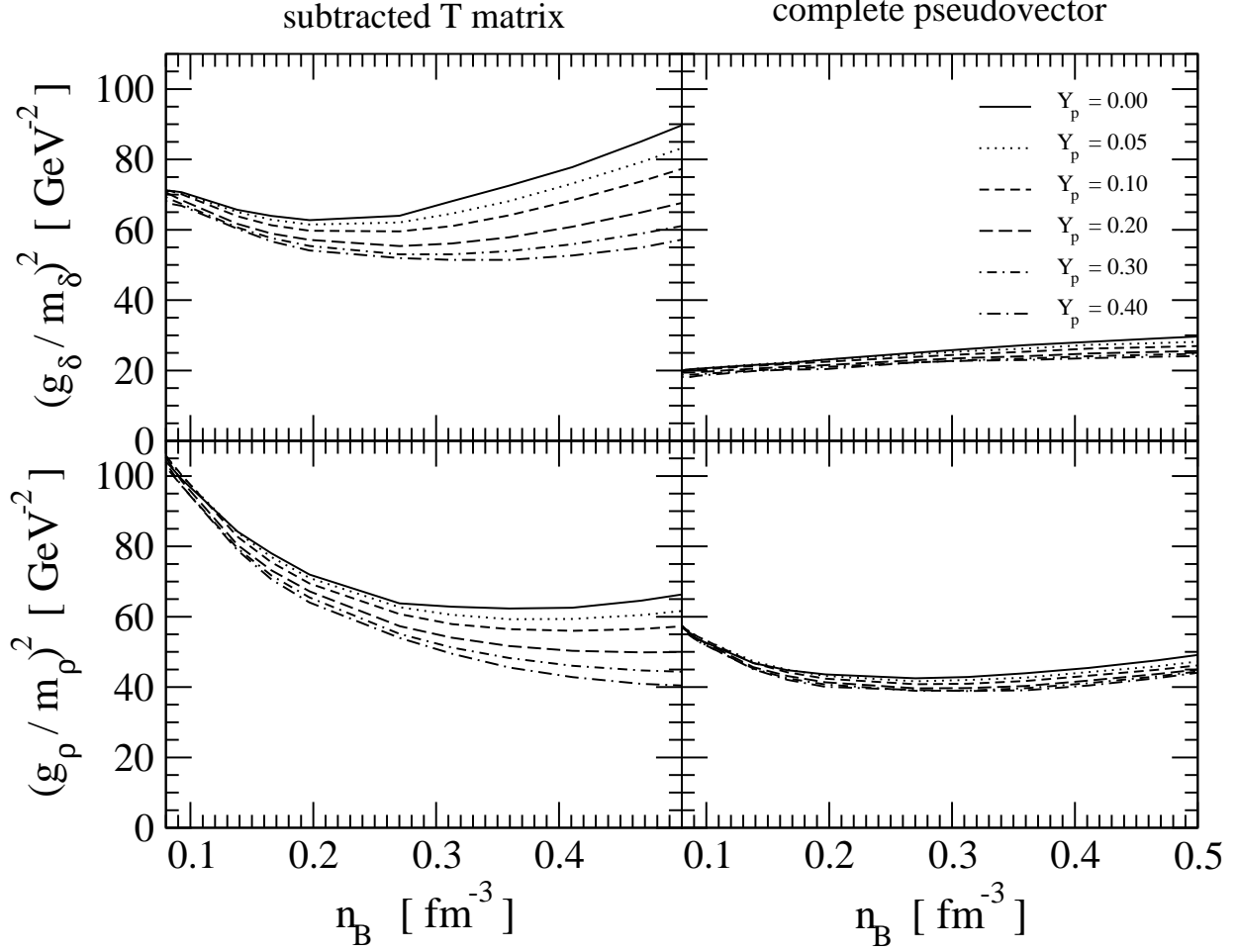


FIG. 7: The effective coupling constants in the isovector scalar g_δ and vector g_ρ as a function of the baryon density for proton fractions Y_p ranging from 0 to 0.4 using the complete pv and subtracted T matrix representation.

tions used are the complete pv representation and subtracted T matrix representation. As already mentioned before, the magnitude of the self-energy depends crucially on the projection scheme which is used for the T matrix. As a consequence the coupling constants are also depending on the projection scheme. For the complete pv representation the strength of the isoscalar coupling constants clearly decreases as the density increases. Applying the subtracted T matrix representation - which is the more reliable method - the density dependence is less pronounced. At low densities, both the scalar g_σ and the vector coupling g_ω show a strong decrease with densities but then the vector coupling stays more or less constant. Such a behavior is qualitatively similar to relativistic mean-field lagrangians which include

non-linear σ self-energy terms. When cast into the form of density dependent couplings these models have a slightly decreasing scalar and a constant vector coupling. However, when applied to finite nuclei the DBHF isoscalar couplings should be renormalized in order to shift the too large saturation density (0.18 fm^{-3} with Bonn A) to the phenomenological value. After such a procedure the isoscalar DBHF self-energy components are in remarkable agreement with the results of [44] based on ChPT + QCD sum rules. A renormalization of the DBHF results can be motivated by higher order corrections of the hole-line expansion, such as e.g. contributions from 3-body forces which are known to shift the saturation density towards smaller values [13].

If DBHF could perfectly be mapped on mean-field phenomenology the isoscalar coupling functions should not depend on the isovector parameter. Since the T-matrix is a complex object where isovector and isoscalar contributions mix such an idealization can not be expected to hold completely. However, the influence of the density on the coupling constants is much larger than that of the proton fraction. For the subtracted T matrix representation, the isoscalar coupling constants show also some dependence on the proton fraction. However, here as well as in the work in Ref. [18] the dependence of the coupling constants on the proton fraction is generally weak. For the subtracted T matrix representation the isoscalar vector channel shows the strongest variation as a function of the proton fraction Y_p which lies in this case between 5 and 10 %.

The strength in the isovector channel is small compared to that in the isoscalar channel, especially for the complete pv representation. Furthermore, a strong dependence on the proton fraction is observed for the subtracted T matrix representation. The results for the isovector channel in case of the subtracted T matrix representation lie closest to the results of Ref. [18] which are based on the Groningen NN interaction. In particular we observe the same increase of the scalar isovector coupling g_δ at large densities. The variation of the isovector couplings as a function of the proton fraction Y_p is generally somewhat larger than observed in [18].

V. SUMMARY AND CONCLUSION

We present a calculation of asymmetric nuclear matter in a relativistic Brueckner framework using the Bonn A potential. The standard treatment, in which the positive-energy-

projected on-shell T matrix has to be decomposed into Lorentz invariant amplitudes, is applied. Furthermore, the T matrix is represented by a set of five linearly independent Lorentz invariants with an average mass for the np interaction. Since the restriction to positive energy states causes on-shell ambiguities concerning the pseudoscalar or pseudovector nature of the interaction [17, 18], some freedom in the choice of the representation exists and the relativistic nuclear self-energy can not be determined in a unique way. This ambiguity is minimized by separating the leading order, i.e. the single-meson exchange, from the full T matrix. Therefore, the contributions stemming from the single- π and- η exchange are given in the complete pv representation. For the other single-meson exchanges and the remaining higher order correlations, the ps representation is chosen.

With this representation scheme, the subtracted T representation scheme [32], we have performed calculations for several observables in asymmetric nuclear matter and compared them with the results for other representation schemes, e.g. the complete pv representation scheme. The binding energy shows the expected quadratic dependence on the asymmetry parameter in both representations. The symmetry energy is found to be 34 MeV at saturation density, whereas in the complete pv representation the value of 37 MeV is found, which is too high. With increasing proton fraction the neutron effective mass increases. In addition, the density dependence is stronger than the asymmetry dependence on the neutron effective mass. Furthermore, a mass splitting of $m_n^* < m_p^*$ is found in both cases.

In summary, Bonn A predicts a nuclear equation of state which is soft for symmetric matter ($K=230$ MeV) but has a stiff isospin dependence ($E_{\text{sym}} = 34$ MeV). Both facts are in agreement with constraints obtained from heavy ion reactions where kaon production can be used to constrain the symmetric part [53] and pion production [54] and isospin diffusion [55] to constrain the symmetry energy .

The results are also analyzed in terms of mean-field Dirac scalar-vector isoscalar-isovector quantities. In general the strength in the isovector channel is small compared to that in the isoscalar channel. However, the found strength in the isovector channel is still significant for the subtracted T matrix. Furthermore, a strong dependence on the proton fraction is observed in that case.

Therefore, the results above have consequences for nuclei with large neutron excess and

for neutron stars.

- [1] K. A. Brueckner, C. A. Levinson, and H. M. Mahmond, *Phys. Rev.* 95 (1954) 217.
- [2] H. A. Bethe, *Phys. Rev.* 103 (1956) 1353.
- [3] J. Goldstone, *Proc. R. Soc. London, Ser. A* 239 (1957) 267.
- [4] H. A. Bethe, *Annu. Rev. Nucl. Sci.* 21 (1971) 93.
- [5] M. I. Haftel and F. Tabakin, *Nucl. Phys. A* 158 (1970) 1.
- [6] D. W. L. Sprung, *Adv. Nucl. Phys.* 5 (1972) 225.
- [7] M. R. Anastasio, L. S. Celenza, W. S. Pong, and C. M. Shakin, *Phys. Rep.* 100 (1983) 327.
- [8] C. J. Horowitz and B. D. Serot, *Nucl. Phys. A* 464 (1987) 613.
- [9] R. Brockmann and R. Machleidt, *Phys. Rev. C* 42 (1990) 1965.
- [10] K. A. Brueckner and S. A. Coon, *Phys. Rev.* 168 (1968) 1184.
- [11] P. J. Siemens, *Nucl. Phys. A* 141 (1970) 225.
- [12] I. Bombaci and U. Lombardo, *Phys. Rev. C* 44 (1991) 1892.
- [13] W. Zuo, I. Bombaci, and U. Lombardo, *Phys. Rev. C* 60 (1999) 024605.
- [14] B. ter Haar and R. Malfliet, *Phys. Rev. Lett.* 59 (1987) 1652; R. Malfliet, *Nucl. Phys. A* 488 (1988) 721c.
- [15] L. Engvik, M. Hjorth-Jensen, E. Osnes, G. Bao, and E. Oestgaard, *Phys. Rev. Lett.* 73 (1994) 2650.
- [16] L. Engvik, E. Osnes, M. Hjorth-Jensen, G. Bao, and E. Oestgaard, *Astrophys. J.* 469 (1996) 794.
- [17] H. Huber, F. Weber, and M. K. Weigel, *Phys. Rev. C* 51 (1995) 1790.
- [18] F. de Jong and H. Lenske, *Phys. Rev. C* 58 (1998) 890.
- [19] C.-H. Lee, T. T. S. Kuo, G. Q. Li, and G. E. Brown, *Phys. Rev. C* 57 (1998) 3488.
- [20] E. Schiller and H. Müther, *Eur. Phys. J. A* 11 (2001) 15.
- [21] D. Alonso and F. Sammarruca, *nucl-th/0301032*.
- [22] M. Prakash and T. L. Ainsworth, *Phys. Rev. C* 36 (1987) 346.
- [23] N. Fröhlich, H. Baier, and W. Bentz, *Phys. Rev. C* 57 (1998) 3447.
- [24] H. A. Bethe, *Rev. Mod. Phys.* 62 (1990) 801.
- [25] C. J. Pethick, D. G. Ravenhall, and C. P. Lorentz, *Nucl. Phys. A* 584 (1995) 675.

- [26] I. Tanihata, *Prog. Part. Nucl. Phys.* 35 (1995) 505; P. G. Hansen, A. S. Jensen, and B. Jonson, *Annu. Rev. Nucl. Part. Sci.* 45 (1995) 591.
- [27] A. E. L. Dieperink, Y. Dewulf, D. Van Neck, M. Waroquier, and V. Rodin, *Phys. Rev. C* 68 (2003) 064307.
- [28] B.-A. Li, C. M. Ko, and Z. Ren, *Phys. Rev. Lett.* 78 (1997) 1644.
- [29] C. Nuppenau, Y. J. Lee, and A. D. MacKellar, *Nucl. Phys. A* 504 (1989) 839.
- [30] L. Sehn, C. Fuchs, and A. Faessler, *Phys. Rev. C* 56 (1997) 216.
- [31] C. Fuchs, T. Waindzoeh, A. Faessler, and D. S. Kosov, *Phys. Rev. C* 58 (1998) 2022.
- [32] T. Gross-Boelting, C. Fuchs, and Amand Faessler, *Nucl. Phys. A* 648 (1999) 105.
- [33] R. Machleidt, *Adv. Nucl. Phys.* 19 (1989) 189.
- [34] B. D. Serot and J. D. Walecka, *Adv. Nucl. Phys.* 16 (1986) 1.
- [35] P. Poschenrieder and M. K. Weigel, *Phys. Rev. C* 38 (1988) 471.
- [36] H. A. Bethe, B. H. Brandow, and A. G. Petschek, *Phys. Rev.* 129 (1963) 225.
- [37] R. H. Thompson, *Phys. Rev. D* 1 (1970) 110.
- [38] B. ter Haar and R. Malfliet, *Phys. Rep.* 149 (1987) 207.
- [39] K. Erkelenz, *Phys. Rep. C* 13 (1974) 191.
- [40] M. Rose, *Elementary Theory of Angular Momentum* (Wiley, New York, 1957).
- [41] J. A. Tjon and S. J. Wallace, *Phys. Rev. C* 32 (1985) 267.
- [42] W. D. Myers and W. J. Swiatecky, *Nucl. Phys. A* 601 (1996) 141.
- [43] T. Nikšić, D. Vretenar, and P. Ring, *Phys. Rev. C* 66 (2002) 064302.
- [44] P. Finelli, N. Kaiser, D. Vretenar, and W. Weise, *Nucl. Phys. A* 735 (2004) 449.
- [45] D. Vretenar, T. Nikšić, P. Ring, *Phys. Rev. C* 68 (2003) 024310.
- [46] B.-A. Li, *nucl-th/0404040*.
- [47] D. M. Patterson, R. R. Doering, and A. Galonsky, *Nucl. Phys. A* 263 (1976) 261.
- [48] R. P. de Vito, S. M. Austin, W. Sterrenburg, and U. E. P. Berg, *Phys. Rev. Lett.* 47 (1981) 628.
- [49] R. de Leo et al., *Phys. Lett. B* 98 (1981) 233.
- [50] K. Kwiatkowski and N. S. Wall, *Nucl. Phys. A* 301 (1978) 349.
- [51] M. Baldo and A. Fiasconaro, *Phys. Lett. B* 491 (2000) 240.
- [52] C. Fuchs, H. Lenske, H.H. Wolter, *Phys. Rev. C* 52 (1995) 3043.
- [53] C. Fuchs, Amand Faessler, E. Zabrodin, Y.M. Zheng, *Phys. Rev. Lett.* 86 (2001) 1974.

- [54] T. GaiTanos, M. Di Toro, S. Typel, V. Baran, C. Fuchs, V. Greco, H. H. Wolter, Nucl. Phys. A732 (2004) 24.
- [55] T. GaiTanos, M. Colonna, M. Di Toro, H. H. Wolter, Phys. Lett. B595 (2004) 209; L.-W. Chen, C.M. Ko, B.-A. Li, nucl-th/0407032.
- [56] From now on we omit the tilde because in the following we normally deal with \tilde{m}_F^* , $\tilde{k}^{*\mu}$.
- [57] We thank M. Di Toro for bringing our attention towards this fact.